Rotationally resolved multiphoton ionization photoelectron spectroscopy of the [a 1 Δ]3dπ 2 Φ and [a 1 Δ]5pπ 2 Φ Rydberg states of the SH radical

J. B. Milan, W. J. Buma, C. A. de Lange, Kwanghsi Wang, and V. McKoy

Citation: The Journal of Chemical Physics **107**, 2782 (1997); doi: 10.1063/1.474635
View online: http://dx.doi.org/10.1063/1.474635
View Table of Contents: http://scitation.aip.org/content/aip/journal/jcp/107/8?ver=pdfcov
Published by the AIP Publishing

Rotationally resolved multiphoton ionization photoelectron spectroscopy of the $[a\ ^1\Delta]3d\pi\ ^2\Phi$ and $[a\ ^1\Delta]5p\pi\ ^2\Phi$ Rydberg states of the SH radical

J. B. Milan, W. J. Buma, and C. A. de Lange
Laboratory for Physical Chemistry, University of Amsterdam, Nieuwe Achtergracht 127, 1018 WS Amsterdam, The Netherlands

Kwanghsi Wang and V. McKoy
Arthur Amos Noyes Laboratory for Chemical Physics, California Institute of Technology, Pasadena, California 91125

(Received 7 March 1997; accepted 14 May 1997)

Experimental and theoretical results on the rotationally resolved photoelectron spectra of the $[a\ ^1\Delta]3d\pi\ ^2\Phi(v'=0)$ and the $[a\ ^1\Delta]5p\pi\ ^2\Phi(v'=0)$ Rydberg states of the SH radical are presented. In particular, for the former state, ionization via a large number of members of different rotational branches is considered. The interplay between experiment and *ab initio* calculations, including alignment, allows for a detailed interpretation of the results. Asymmetries apparent in the rotational ionic distributions and the observed suppression of transitions involving a large change in angular momentum can be explained on the basis of the theory. © *1997 American Institute of Physics.* [S0021-9606(97)04831-9]

I. INTRODUCTION

Although the mercapto radical (SH) has been studied with various spectroscopic techniques over the past several decades, information on its excited electronic states is still relatively scarce. The electronic absorption spectrum of SH has been investigated from the near ultraviolet into the vacuum ultraviolet region, and ten electronic transitions, all arising from the ground state, have been identified.[1–3]

SH is a molecule of environmental importance and plays a role in the ultraviolet photochemistry of various sulphur-containing compounds which are released into the earth's atmosphere from natural and anthropogenic sources. In view of its electronic similarity to the abundant OH radical, the mercapto radical may well have astrophysical relevance.[4] Several sulphur-containing molecules have already been observed in interstellar space, but despite serious attempts to detect SH,[5,6] the molecule until now has remained elusive under extraterrestial conditions.

The $X\ ^2\Pi$ ground state of SH possesses a $(1\sigma)^2(2\sigma)^2(3\sigma)^2(1\pi)^4(4\sigma)^2(5\sigma)^2(2\pi)^3$ electronic configuration. Due to spin-orbit interaction the ground state shows an inverted splitting with the $^2\Pi_{3/2}$ state below the $^2\Pi_{1/2}$ component.[7] The ground state of the radical has been well characterized through studies of the Λ-doubling, vibrational–rotational, and pure rotational transitions.[8] The partly filled 2π molecular orbital is essentially a nonbonding $3p$ atomic orbital on the sulphur atom. Ionization from this orbital leads to three different ionic states, viz. $X\ ^3\Sigma^-$, $a\ ^1\Delta$, and $b\ ^1\Sigma^+$, located at 10.421, 11.645, and 12.76 eV, respectively, above the ground state of the neutral radical.[9–11]

To obtain detailed information about the spectroscopy and the dynamics of molecular excited states, resonance enhanced multiphoton ionization in conjunction with photoelectron spectroscopy (REMPI-PES) is nowadays the method of choice. From a chemical point of view, an important advantage of REMPI-PES is its unique capability of providing direct experimental information about configuration interaction and vibronic coupling.[12–15] Picosecond time-resolved photoionization pump–probe experiments in combination with photoelectron spectroscopy also provide valuable real-time information about the dynamics of molecular excited states.[16] Furthermore, the application of REMPI-PES is not limited to stable molecules. In particular, the versatility, selectivity, and sensitivity of the technique allow its application to a variety of radical species.[12,17–24] REMPI-PES has already been successfully applied to our title radical SH. The focus of these studies has been on excited states which belong to the Rydberg series which do not converge to the ionic ground state, but rather to excited ($a\ ^1\Delta$ and $b\ ^1\Sigma^+$) ionic states. Cases in point are the $[a\ ^1\Delta]3d\pi\ ^2\Phi$ Rydberg state located just below the lowest ionic limit, and the $[a\ ^1\Delta]5p\pi\ ^2\Phi$ Rydberg state, which lies above the $X\ ^3\Sigma^-$ ionic state.[25] In addition, a large number of hitherto undetected Rydberg levels, also with excited ionic cores, have been the subject of a separate publication.[26]

When REMPI-PES on radicals is performed with sufficiently high resolution, rotationally resolved studies on these elusive species provide an abundance of detailed information pertaining to the dynamics of the photoionization process under consideration. The first rotationally resolved REMPI-PES study involving the ionic ground state of a radical was carried out on OH.[18] Results of preliminary studies of rotationally resolved REMPI-PES of the $[a\ ^1\Delta]3d\pi\ ^2\Phi$ core-excited Rydberg state of the SH radical have recently been reported.[27] In addition, a pulsed-field ionization with zero-kinetic-energy electron detection (ZEKE-PFI) study, involving for the first time an excited ionic state of a radical species, has been carried out via the same state of SH.[11]

The present paper is concerned with a detailed account

 0021-9606/97/107(8)/2782/11/$10.00

of the rotationally resolved photoelectron spectroscopy of the $[a\ ^1\Delta]3d\pi\ ^2\Phi(v'=0)$ and the $[a\ ^1\Delta]5p\pi\ ^2\Phi(v'=0)$ Rydberg states of the SH radical. From these REMPI-PES results a wealth of dynamical information on the photoionization process will be derived. Extensive research has previously shown that the interplay between rotationally resolved photoelectron spectroscopy and sophisticated *ab initio* quantum-chemical calculations can be particularly fruitful.[18,20,24,27,28] By combining an advanced theoretical treatment with experimental results on the $[a\ ^1\Delta]3d\pi\ ^2\Phi$ and $[a\ ^1\Delta]5p\pi\ ^2\Phi$ Rydberg states of SH, the value of this approach will be further illustrated.

II. EXPERIMENT

The experimental setup has been described in detail elsewhere.[13,24] SH radicals were predominantly generated in their electronic and vibrational ground states by photolysis of H_2S through single-photon excitation to the first dissociative absorption band which spans the wavelength range 180–270 nm. Photons for both the photolysis and the subsequent spectroscopy of the SH radicals were produced using an excimer-pumped dye laser system. Wavelength and photoelectron kinetic energy calibrations were performed using resonances of xenon and atomic sulphur (which is also a product of the photolysis of H_2S and SH) in the two-photon energy range of 79 500–89 800 cm^{-1}. Because of different experimental conditions, the spectral resolution amounted to approximately 12 meV for the $[a\ ^1\Delta]3d\pi\ ^2\Phi$ state and to approximately 25 meV for the $[a\ ^1\Delta]5p\pi\ ^2\Phi$ state. In order to keep track of the various fragmentation processes, the magnetic bottle spectrometer could also be operated in the time-of-flight ion detection mode. Peaks due to S^+, SH^+, and H_2S^+ could be easily separated. H_2S (99.6%, Messer Griesheim) was used without further purification and was introduced into the spectrometer as a continuous effusive ''leak.''

III. THEORY AND CALCULATION

A. Differential cross section

The general theory of molecular REMPI processes used in the present studies has been described previously.[29,30] Here we present only a brief outline of some essential features of this approach as it is used to obtain rotational ion distributions for SH^+ resulting from $(2+1)$ REMPI of SH via the $[a\ ^1\Delta]3d\pi\ ^2\Phi$ and $[a\ ^1\Delta]5p\pi\ ^2\Phi$ Rydberg states. For linearly polarized light, ionization originating from each of the $(2J+1)$ magnetic sublevels of the initial state forms an independent channel. The total cross section σ for ionization of a J level of the initial state leading to a J_+ level of the ion can be written as

$$\sigma \propto \sum_{\substack{lm \\ M_J, M_{J_+}}} \rho_{M_J,M_J} |C_{lm}(M_J, M_{J_+})|^2, \tag{1}$$

where ρ_{M_J,M_J} is the population of a specific M_J level of the intermediate state created by two-photon excitation. For the transitions investigated in the present paper, ρ_{M_J,M_J} is a product of a 3-j symbol and a rotational line strength B,[31]

$$\rho_{M_J,M_J} = \mathcal{N} \begin{pmatrix} J & 2 & J_0 \\ -M_J & 0 & M_J \end{pmatrix}^2 B, \tag{2}$$

where $\mathcal{N}$ is a normalization constant.

The $C_{lm}(M_J, M_{J_+})$ coefficients of Eq. (1) are related to the probability for photoionization of the M_J level of the intermediate state leading to the M_{J_+} level of the ionic state. The $C_{lm}(M_J, M_{J_+})$ coefficients, which explicitly consider the spin coupling associated with multiplet-specific final-state wave functions and an intermediate coupling scheme between Hund's cases (a) and (b) for the initial and ionic states, have the simple form:[29]

$$\begin{aligned} &C_{lm}(M_J, M_{J_+}) \\ &= C'[1+(-1)^Q]\Bigg[\sum \widetilde{I}_{l\lambda\mu;\Sigma_e} G \begin{pmatrix} J_+ & J & J_t \\ -\Omega_+ & \Omega & \lambda_t \end{pmatrix} \\ &\quad \times \begin{pmatrix} S_+ & 1/2 & S \\ \Sigma_+ & \Sigma_e & -\Sigma \end{pmatrix} + \widetilde{I}_{l\lambda\mu;\Sigma_e} \\ &\quad \times (-1)^P G \begin{pmatrix} J_+ & J & J_t \\ -\Omega_+ & -\Omega & \lambda_t \end{pmatrix} \\ &\quad \times \begin{pmatrix} S_+ & 1/2 & S \\ \Sigma_+ & \Sigma_e & \Sigma \end{pmatrix} \Bigg], \end{aligned} \tag{3}$$

where

$$G = \begin{pmatrix} J_r & 1 & J_t \\ -\lambda_r & \mu & -\lambda_t \end{pmatrix} \begin{pmatrix} 1/2 & l & J_r \\ -\Sigma_e & -\lambda & \lambda_r \end{pmatrix}, \tag{4}$$

$$Q = \Delta J + \Delta S + \Delta p + l, \tag{5}$$

$$p = \begin{cases} 0 & \text{for } e \text{ states} \\ 1 & \text{for } f \text{ states,} \end{cases} \tag{6}$$

and

$$\widetilde{I}_{l\lambda\mu;\Sigma_e} = \sum_{\Lambda_f \Sigma_f} \langle \Lambda_+ \lambda | \Lambda_f \rangle \langle \Sigma_+ \Sigma_e | \Sigma_f \rangle I_{l\lambda\mu}(\Lambda_f \Sigma_f), \tag{7}$$

with $\Delta J = J_+ - J$, $\Delta S = S_+ - S$, $\Delta p = p_+ - p$. In Eq. (3), C' is a laboratory-frame quantity given in Ref. 29. In these equations, Ω denotes the component of total electronic angular momentum about the internuclear axis, Λ the projection of electronic orbital angular momentum along the internuclear axis, S the total spin, Σ its projection along the internuclear axis, Σ_e the projection of the spin of the photoelectron along the laboratory z axis, and p the parity of each rotational level. Equations (3) and (5) yield the parity selection rule[29,32,33]

$$\Delta J + \Delta S + \Delta p + l = \text{even} \tag{8}$$

for photoionization of both Rydberg states of SH. Since each rotational level of the Rydberg and ionic states of SH studied

here contains both e and f parities, each rotational transition involves contributions from both even and odd partial waves of the photoelectron matrix element.

A central quantity in this study is the matrix element, $I_{l\lambda\mu}$ of Eq. (7), for photoejection of an electron from a bound molecular orbital into the electronic continuum. In the single-particle picture, the photoelectron matrix element of Eq. (7) for photoionization of an orbital ϕ_i in the molecular frame can be written as

$$I_{l\lambda\mu}=(-i)^l e^{i\eta_l}\int dR\ \chi^*_{v_+}(R) r^{l\lambda\mu}_{fi}(R)\chi_{v_i}(R), \tag{9}$$

where

$$r^{l\lambda\mu}_{fi}(R)=\sum_{l',l_0}\langle\Psi_{ll'\lambda}(k,r,R)Y_{l'\lambda}(\hat{\mathbf{r}}')| \times rY_{1\mu}(\hat{\mathbf{r}}')|\phi_{il_0}(r,R)Y_{l_0,\lambda_0}(\hat{\mathbf{r}}')\rangle, \tag{10}$$

with η_l the Coulomb phase shift, and $\Psi_{ll'\lambda}$ the partial wave component of the photoelectron orbital[30] with momentum $\mathbf{k}$. Which partial waves l are dominant depends on how l' and l are coupled via the molecular ion potential. This l coupling in the photoelectron wave function, in turn, influences the ion rotational distribution.

B. Multiplet-specific wave functions and potentials

There are three dipole-allowed final-state wave functions $|\Lambda_f\Sigma_f\rangle$ for photoionization of the $3d\pi$ (or $5p\pi$) orbital of the $[a\ ^1\Delta]3d\pi\ ^2\Phi$ (or $[a\ ^1\Delta]5p\pi\ ^2\Phi$) Rydberg state of SH. An electron can be ejected from this Rydberg orbital into the $k\sigma$, $k\pi$, or $k\delta$ continuum channel. Ejection through the $k\sigma$, $k\pi$, and $k\delta$ continua results in an electron-ion complex which has $^2\Delta$, $^2\Phi$, and $^2\Gamma$ total final state symmetry, respectively. The final-state wave functions are

$$\Psi(^2\Delta)=(\text{core})2\pi^2_+ k\sigma^1, \tag{11}$$

$$\Psi(^2\Phi)=(\text{core})2\pi^2_+ k\pi^1_+, \tag{12}$$

and

$$\Psi(^2\Gamma)=(\text{core})2\pi^2_+ k\delta^1_+, \tag{13}$$

where $(\text{core})=1\sigma^2 2\sigma^2 3\sigma^2 1\pi^4 4\sigma^2 5\sigma^2$.

Within the frozen-core Hartree–Fock model, the one-electron Schrödinger equation for the photoelectron orbital ϕ_k associated with these final-state wave functions can be shown to have the form[30]

$$P\left(f+\sum_{i=\text{core}}(2J_i-K_i)+a_nJ_n+b_nK_n-\epsilon\right)P|\phi_k\rangle=0, \tag{14}$$

where J_i and K_i are the Coulomb and exchange operators, respectively, and P is a projection operator which enforces orthogonality of the continuum orbital to the occupied orbitals. The photoelectron kinetic energy is given by $\epsilon=(1/2)k^2$. The one-electron operator f in Eq. (14) is

$$f=-\frac{1}{2}\nabla^2_i-\sum_\alpha\frac{Z_\alpha}{r_{i\alpha}}, \tag{15}$$

where Z_α is a nuclear charge. Using the final-state wave functions of Eqs. (11)–(13), the coefficient a_n and b_n associated with the $2\pi_+$ orbital assume values of -1 and -1, respectively. The corresponding values for the $2\pi_-$ orbital are 0 and 0.

C. Numerical details

For the wave functions of the $[a\ ^1\Delta]3d\pi\ ^2\Phi(2\pi\rightarrow4\pi)$ and $[a\ ^1\Delta]5p\pi\ ^2\Phi(2\pi\rightarrow5\pi)$ Rydberg states, we use the improved virtual orbital (IVO) method,[34] in which the core orbitals are taken to be those of the fully relaxed, excited $^1\Delta(2\pi^{-1})$ ion, and the $3d\pi$ (4π) and $5p\pi$ (5π) orbitals are obtained as eigenfunctions of the one-electron Schrödinger equation containing the static-exchange potential, V_{N-1}, of this core. The wave function of the $a\ ^1\Delta$ ionic state is obtained at the self-consistent-field (SCF) level. The orbital basis used in these calculations consists of a $[6s4p]$ contraction of the $(12s9p)$ primitive Cartesian functions of McLean and Chandler,[35] augmented with one s $(\alpha=0.06)$ and three d $(\alpha=1.0,\ 0.25,$ and $0.06)$ functions on the sulfur atom. On the hydrogen atom, we used a $[3s1p]$ contraction of the $(4s2p)$ primitive basis of Dunning,[36] augmented with three s $(\alpha=0.035,\ 0.008,$ and $0.0025)$ and three p $(\alpha=0.25,\ 0.1,$ and $0.05)$ functions. This basis is further augmented with four s $(\alpha=0.02,\ 0.01,\ 0.001,$ and $0.0002)$, four p $(\alpha=0.012,\ 0.002,\ 0.0001,$ and $0.000\,02)$, and three d $(\alpha=0.01,\ 0.0025,$ and $0.000\,35)$ functions on the center of mass. At an internuclear distance of 2.6 a.u., the SCF energies of the $[a\ ^1\Delta]3d\pi\ ^2\Phi$ and $[a\ ^1\Delta]5p\pi\ ^2\Phi$ Rydberg states were $-397.757\,750$ and $-397.738\,114$ a.u., respectively. The $3d\pi$ orbital has a single-center expansion of 5.04% p, 94.51% d, and 0.09% f character about the center of mass, while the $5p\pi$ orbital has 92.63% p, 7.30% d, and 0.07% f character.

To obtain the photoelectron orbitals, ϕ_k, we have used an iterative procedure, based on the Schwinger variational principle, to solve the Lippmann–Schwinger equation associated with Eq. (14). Details of this procedure are given in Ref. 30.

IV. RESULTS AND DISCUSSION

A. Photoionization of the $3d\pi$ orbital

Figure 1 shows the two-photon excitation spectrum of the SH radical in the two-photon energy range of $77\,500$–$78\,500\ \text{cm}^{-1}$ obtained by only monitoring photoelectrons with a kinetic energy of approximately 2.9 eV. These electrons derive from a core-preserving photoionization process in which a $(2+1)$ photon transition from the $X\ ^2\Pi(v''=0)$ ground state to the $a\ ^1\Delta(v^+=0)$ excited ionic state occurs. At the two-photon level, resonance enhancement via the $[a\ ^1\Delta]3d\pi\ ^2\Phi(v'=0)$ Rydberg state takes place. Assignments of the transitions belonging to the various rotational branches are presented by combs above the experimental spectra. Spectra obtained by time-of-flight ion detection in which SH^+ ions are monitored are essentially identical to those measured with electron detection, thus con-

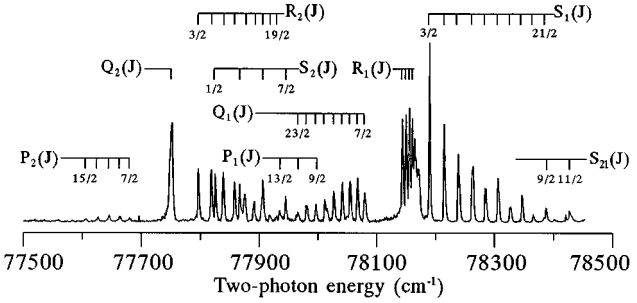

FIG. 1. The two-photon excitation spectrum of the SH radical in the two-photon energy range of 77 500–78 500 cm^{-1} obtained by only monitoring photoelectrons with a kinetic energy of approximately 2.9 eV. These electrons derive from a $(2+1)$ photon transition from the $X\ ^2\Pi(v''=0)$ ground state to the $a\ ^1\Delta(v^+=0)$ excited ionic state via the $[a\ ^1\Delta]3d\pi\ ^2\Phi$.

firming the above assignments. The excitation spectra show clear substructure with energy separations corresponding to the well-known spin-orbit splitting of the ground state $[A_0''(\mathrm{SH})=-376.835\ \mathrm{cm}^{-1}]$.[7] The excitation spectrum of Fig. 1 also shows extensive rotational structure. Details of the rotational analyses are given elsewhere;[26] the relevant parameters for this state are summarized in Table I.

Figure 2 shows the measured (left column) and calculated (right column) photoelectron spectra obtained in a $(2+1)$ photoionization process via the $S_{11}(3/2)$ to $S_{11}(11/2)$, $S_{11}(15/2)$, and $S_{11}(19/2)$ rotational branches of the $[a\ ^1\Delta]3d\pi\ ^2\Phi \leftarrow\leftarrow X\ ^2\Pi$ two-photon transition of the SH radical leading to the $a\ ^1\Delta$ excited ionic state of SH^+. Our experiments have established that ionization only takes place to the $a\ ^1\Delta(v^+=0)$ excited ionic level. No transitions corresponding to higher vibrational levels of the $a\ ^1\Delta$ state, nor to the $X\ ^3\Sigma^-$ ground ionic state and the energetically accessible $b\ ^1\Sigma^+$ higher ionic state were observed. From the spectra it is also apparent that the amount of resolved rotational structure increases drastically as the photoelectron spectra are measured via rotational lines corresponding to higher rotational quantum numbers in the intermediate $^2\Phi$ state. The calculated spectra were convoluted with a Gaussian detector function with a full width at half-maximum (FWHM) of 12 meV. Possible effects on the rotational ion distributions of alignment in the ground state of SH fragments resulting from the H_2S photodissociation step have been neglected in our calculations. However, the effects of alignment following the two-photon absorption to the excited $^2\Phi$ state have been included via the ρ_{M_j,M_j} of Eq. (2). Since the e/f parities of the rotational levels in the $^2\Phi$ intermediate state and the $a\ ^1\Delta$ ionic state cannot be resolved experimentally, the contributions to the cross sections from both the e and f parities of each rotational level have been summed up in the calculated spectra.

TABLE I. Spectroscopic constants for the two $^2\Phi$ Rydberg state of SH (Refs. 24 and 25). For comparison, the spectroscopic constants of the $X\ ^2\Pi$ ground state are given as well (Ref. 7).

Electronic state	T_0	B_0	$D_0\times10^{-4}$	A_0
$X\ ^2\Pi$	0	9.604	4.8299	−376.835
$[a\ ^1\Delta]3d\pi\ ^2\Phi$	78 006.36	8.855	2.9	−1.18
$[a\ ^1\Delta]5p\pi\ ^2\Phi$	85 277.6	8.350	−0.8	−0.42

Agreement between the calculated and measured spectra of Fig. 2 is excellent. Both show important features upon photoionization of this $3d\pi$ orbital. In Fig. 2 both calculated and measured spectra show only small changes in total angular momentum, $|\Delta N|\leqslant 2$, for every rotational branch. From conservation of angular momentum, the observation of transitions with $|\Delta N|\leqslant 2$ suggests that the photoelectron continua are dominated by the $s(l=0)$ and $p(l=1)$ partial waves. This differs from expectations on the basis of atomiclike propensity rules since p and f partial waves would be expected for photoionization of the $3d\pi$ orbital with its 95% d character.

To understand the underlying dynamics of these rotationally resolved photoelectron spectra, it is useful to examine the angular momentum composition of the photoelectron matrix element. Figure 3 shows the magnitude of the (incoming-wave normalized) partial wave dipole amplitude $|D_l^{(-)}|$ as a function of photoelectron kinetic energy for the photoionization channels $3d\pi\rightarrow k\sigma$ [Fig. 3(a)], $3d\pi\rightarrow k\pi$ [Fig. 3(b)], and $3d\pi\rightarrow k\delta$ [Fig. 3(c)] via the $[a\ ^1\Delta]3d\pi\ ^2\Phi$ Rydberg state of SH. A dominant $f(l=3)$ wave is clearly seen in all three ($k\sigma$, $k\pi$, and $k\delta$) continuum channels. The relatively weak p wave in both the $k\sigma$ and $k\pi$ channels near threshold may indicate the presence of a Cooper zero in the discrete region. On the other hand, a Cooper minimum is seen in the $d(l=2)$ wave of the $k\delta$ channel around 1.5 eV. The effects of this Cooper minimum on the rotational ion distributions may be weak since its amplitude is relatively small compared to that of the f wave. That such large changes (up to $\Delta N=\pm 4$) in angular momentum are not seen in these spectra, in spite of the significant magnitude of the f angular momentum component of the photoelectron matrix element, is due to interference between the f waves in the different photoelectron continua. To test this assumption, we arbitrarily varied the phase factor of the f-wave contribution in one of the three (σ, π, and δ) continuum channels and the resulting spectra show strong $\Delta N=\pm 3$ and ± 4 transitions. It is interesting to point out that this interference effect in the photoelectron matrix element is evident over a broad energy range.

While interference between f waves of the different continua results in extremely weak $\Delta N=\pm 3$ and ± 4 peaks, more than 99% of the spectral population still arises from the f wave. On the other hand, the angular distributions of the photoelectron behave quite differently. For example, Fig. 4 shows the photoelectron angular distributions resulting from $(2+1)$ REMPI via the $S_{11}(19/2)$ branch of the $[a\ ^1\Delta]3d\pi\ ^2\Phi$ state of SH. It is interesting that none of the angular distributions shows strong f-wave behavior in spite of its dominance in the photoionization process. The photoelectron angular distributions are also dependent on the rotational level of the ion, indicating that they result from different partial wave components of the photoelectron matrix element. Similar behavior is also seen in other rotational branches.

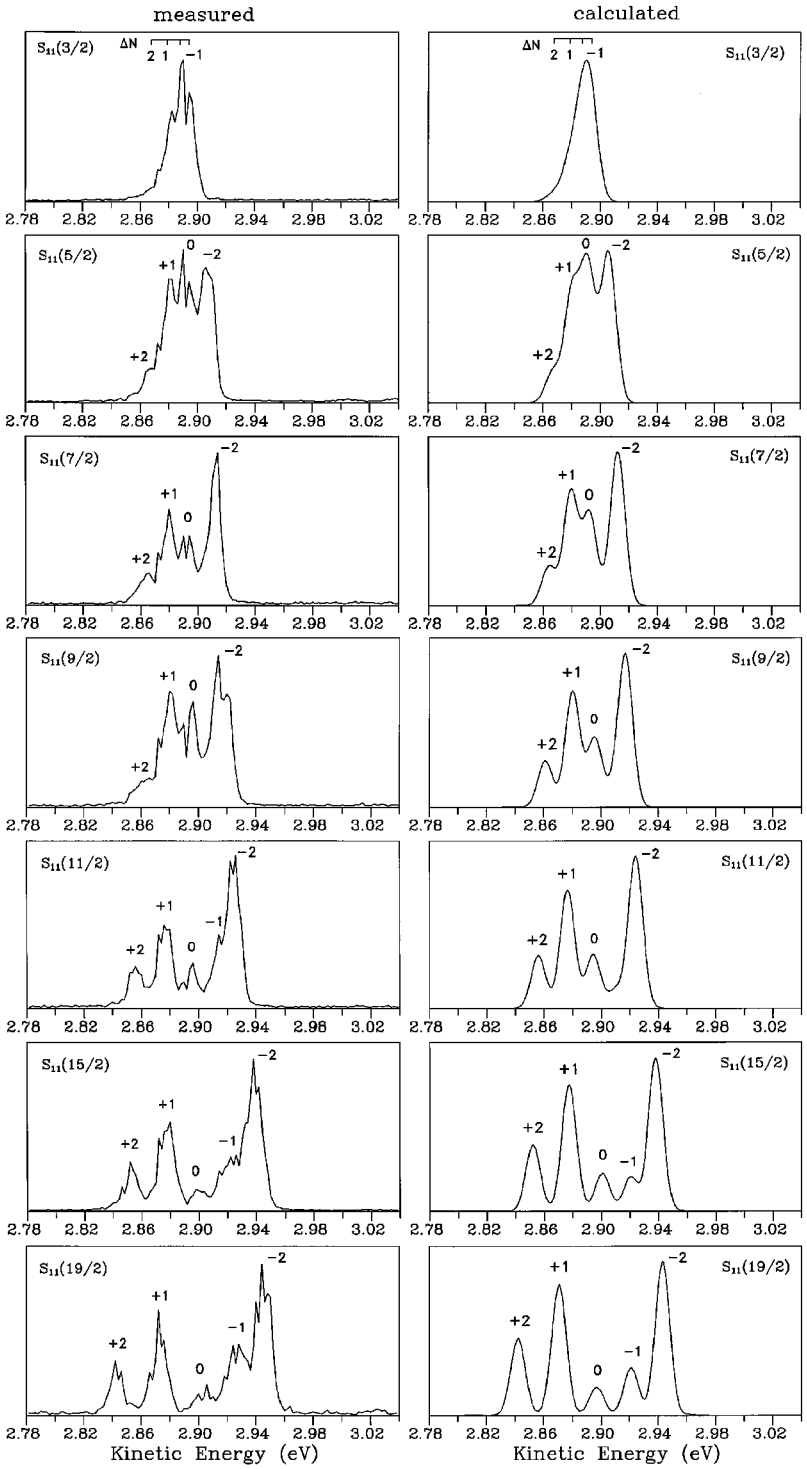

FIG. 2. The measured (left column) and calculated (right column) photoelectron spectra obtained in a $(2+1)$ photoionization process via the $S_{11}(3/2)$ to $S_{11}(11/2)$, $S_{11}(15/2)$, and $S_{11}(19/2)$ rotational lines of the $[a\ ^1\Delta]3d\pi\ ^2\Phi \leftarrow\leftarrow X\ ^2\Pi$ two-photon transition of the SH radical leading to the $a\ ^1\Delta$ excited ionic state of the SH^+. The labeling denotes the changes in rotational angular momentum ΔN.

Figure 2 also illustrates the character of the angular momentum transfer taking place as a function of rotational quantum numbers. For example, at smaller N' rotational levels of the $[a\ ^1\Delta]3d\pi\ ^2\Phi$ state, such as $N'=3$ [via the $S_{11}(3/2)$ branch], the photoionization process favors no angular momentum transfer, i.e., $\Delta N=0$. At larger N' [$N'=11$ via the $S_{11}(19/2)$ branch], the transition favors larger angular momentum transfers such as $\Delta N=\pm 1$ and $\Delta N=\pm 2$. The tendency for decreasing intensity for the $\Delta N=0$ transitions as the rotational quantum numbers increase is very apparent here. Also, the most intense transition in Fig. 2 for all the rotational branches is the $\Delta N=-2$ peak except, of course, for the smallest rotational quantum number via the $S_{11}(3/2)$ line where such a transition cannot occur. These

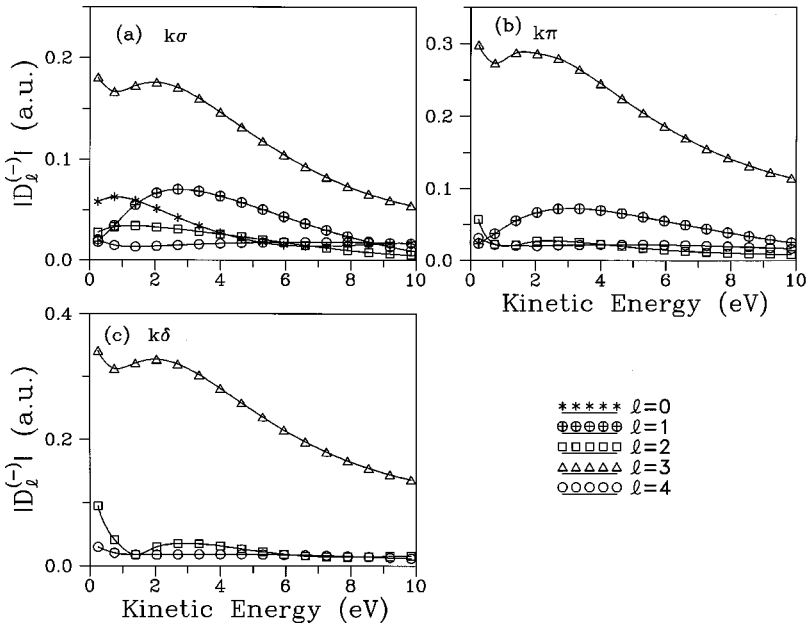

FIG. 3. Magnitude $|D_\ell^{(-)}|$ of the partial wave components of the photoelectron matrix element for photoionization of the $[a\ ^1\Delta]3d\pi\ ^2\Phi$ Rydberg state of SH for the (a) $3d\pi \rightarrow k\sigma$, (b) $3d\pi \rightarrow k\pi$, and (c) $3d\pi \rightarrow k\delta$ ionization channels.

differences between different rotational levels arise from angular momentum coupling.

The most striking features of these photoelectron spectra are the strong asymmetries between the $\Delta N = \pm 1$ transitions and between the $\Delta N = \pm 2$ peaks. Even though slight discrepancies in intensities are expected in many molecular systems, such a large difference in intensities for losing or gaining the same angular momentum upon ionization is highly unusual. This phenomenon is especially evident at smaller rotational quantum numbers of the intermediate $^2\Phi$ state. Since the resonant $^2\Phi$ state has a large component of electronic orbital angular momentum ($\Lambda' = 3$) along the internuclear axis, it could play an important role in these asymmetries. To reach the classical limit for large Λ' requires a correspondingly larger rotational angular momentum. In this limit, one would expect an almost symmetrical spectral profile for high rotational levels. To test this idea, we have also calculated the photoelectron spectra for rotational levels up to $N' = 50$. Indeed, the spectra revealed very symmetrical patterns at such high N's. Therefore, the present study represents a situation which is rather different from that described by the classical picture of rotational motion.

Figure 5 shows the measured (left column) and calculated (right column) photoelectron spectra obtained in a $(2+1)$ photoionization process via the $Q_{11}(7/2)$ to $Q_{11}(23/2)$ rotational branches of the $[a\ ^1\Delta]3d\pi\ ^2\Phi \leftarrow\leftarrow X\ ^2\Pi$ two-photon transition of the SH radical leading to the $a\ ^1\Delta$ excited ionic state of the SH^+. Each photoelectron spectrum is associated with a single rotational branch, except for the $Q_{11}(19/2)$ branch, which was mixed with the $P_{11}(9/2)$ branch. For this mixed branch, the $\Delta N = 0$ peak is unusually intense, which is mainly due to the contribution of the $P_{11}(9/2)$ branch. Again, agreement between the calculated and measured spectra is very encouraging. Both calculated and measured spectra reveal the same unusual spectral behavior seen in Fig. 2 for the S branches.

Since our calculations for the S and Q branches make use of the same photoelectron matrix element, the different spectral profile for the N' rotational level of the $^2\Phi$ intermediate state is primarily due to the different alignment in the N' rotational level induced by the two-photon excitation step. In our calculations, the most intense transition for these Q rotational branches is for the $\Delta N = +1$ peak, except for smaller rotational levels where the $\Delta N = 0$ transitions dominate. However, in the measured spectra the most intense transition is $\Delta N = -1$ for the $Q_{11}(7/2)$ branch, $\Delta N = +1$ for the $Q_{11}(9/2)$ and $Q_{11}(11/2)$ branches, and $\Delta N = -2$ for the other branches. Similar deviations in the intensities of the positive ΔN changes can be observed for the transitions via the S branch. Reasons for these differences between the calculated and measured spectra are not clear.

As can be seen from the above, the agreement between the experimental results and the detailed *ab initio* calculations is extremely satisfactory. On a more approximate level, it is of interest to establish whether a single underlying physical process could explain the main features of the photoelectron spectra of the $[a\ ^1\Delta]3d\pi\ ^2\Phi$ Rydberg state of SH. With hindsight, the results of the *ab initio* calculations can be interpreted in terms of a simple sudden approximation model in which the $a\ ^1\Delta$ ion core acts as a spectator as the $3d\pi$ Rydberg electron is ionized by the absorption of a single photon. In such a model, the angular momentum of the photon is transferred only to the Rydberg electron. Hence, l_0 of the Rydberg orbital should be decoupled from the total angular momentum N [in Hund's case (b) coupling]. This is equivalent to transforming the molecular Hund's case (b) state $|N,\Lambda,M_N\rangle$ with Λ and M_N the angular momentum projections on the molecular and laboratory frames, respec-

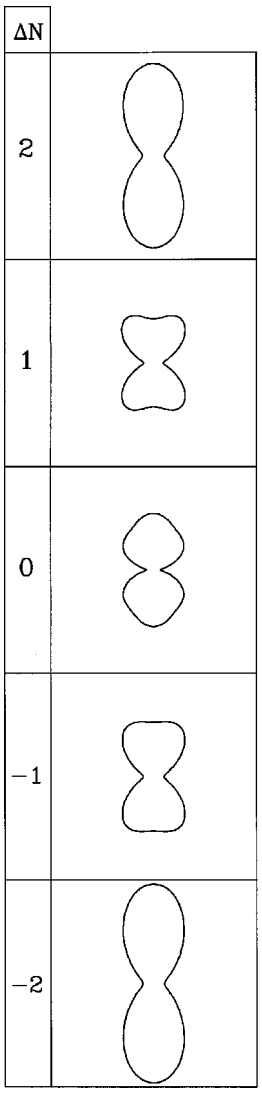

FIG. 4. Calculated photoelectron angular distributions for rotational levels in the $S_{11}(19/2)$ rotational branch of Fig. 2. The polarization direction is vertical ($\theta=0$).

tively, into Hund's case (d) states for which the angular momentum quantum numbers of the ion N_+, Λ_+, and M_{N_+} are well defined. Under these circumstances, we have $l=l_0\pm 1$. In general, the photoionization matrix element for each of the partial waves is proportional to

$$\sum_{k=l\pm 1}(2N+1)(2N_++1)\begin{pmatrix} N & k & N_+ \\ \Lambda & \Lambda_+-\Lambda & -\Lambda_+ \end{pmatrix}^2 |\tilde{r}(k)|^2, \tag{16}$$

where $|\tilde{r}(k)|^2$ is the square of the reduced multipole moment matrix element.[37] For the case of the $[a\ ^1\Delta]3d\pi\ ^2\Phi$ Rydberg state, our calculations show that only the $l=3$ wave plays an important role here. It is apparent that the $k=2$ term is responsible for $\Delta N\leqslant 2$ transitions while the $k=4$ term leads to the higher ΔN transitions. With our calculated photoelectron matrix elements, the contribution from the $k=4$ term, arising from the rescattering process, essentially vanishes due to interference. This leads to a photoionization matrix element proportional to

$$(2N+1)(2N_++1)\begin{pmatrix} N & 2 & N_+ \\ 3 & -1 & -2 \end{pmatrix}^2, \tag{17}$$

which accounts for the observed ΔN changes and branching ratios quite well. Even though this single $k=2$ term of Eq. (16) can approximately describe the measured spectra for the $[a\ ^1\Delta]3d\pi\ ^2\Phi$ state, use of a single term in Eq. (16) in other cases where just one partial wave may also be dominant is justified only if the other term in Eq. (16) vanishes due to interference. Furthermore, Eq. (16) cannot be used in cases where more than a single l contributes to the cross section.

B. Photoionization of the $5p\pi$ orbital

In Fig. 6 we present the two-photon excitation spectrum of the SH radical in the two-photon energy range of 84 715–85 715 cm^{-1} obtained by only monitoring photoelectrons with a kinetic energy of about 4.2 eV. These electrons arise from a core-preserving photoionization process in which a $(2+1)$ photon transition from the $X\ ^2\Pi$ $(v''=0)$ ground state into the $a\ ^1\Delta$ $(v^+=0)$ excited ionic state via the $[a\ ^1\Delta]5p\pi\ ^2\Phi$ $(v'=0)$ Rydberg state occurs. Assignments of the transitions belonging to the various rotational branches are presented by combs above the experimental spectra. Details of the rotational analyses are given in another paper.[25] The relevant parameters for this $5p\pi$ state are also summarized in Table I.

Figure 7 shows the measured [Fig. 7(a)] and calculated [Fig. 7(b)] photoelectron spectra obtained in a $(2+1)$ REMPI photoionization process via the $S_{11}(13/2)+R_{21}(13/2)$ mixed rotational lines of the $[a\ ^1\Delta]5p\pi\ ^2\Phi(v'=0)\leftarrow\leftarrow X\ ^2\Pi$ two-photon transition of the SH radical leading to the $a\ ^1\Delta$ excited ionic state. The calculated spectrum has been convoluted with a Gaussian detector function with an FWHM of 15 meV, which is smaller than our experimental resolution of $\sim$25 meV, but serves to distinguish the individual rotational transitions. This excited Rydberg state has been characterized before,[25] and is peculiar in the sense that it is located above the lowest ionization limit. The photoelectron spectra show partially resolved ionic rotational structure for ionization via the higher rotational quantum numbers of the intermediate state. Since the $^2\Phi$ state is well described by Hund's case (b), both transitions access the same N' level. The photoelectron profile for each excitation transition will be almost the same except for minor differences induced by the alignment. Agreement between the calculated and measured spectra is still good except for smaller kinetic energies. The reason for this discrepancy is not clear.

The largest changes in rotational angular momentum here are for $|\Delta N|\leqslant 2$, which is the same as for photoionization of the $3d\pi$ orbital. On the basis of atomiclike selection rules, one would expect a dominant d wave for photoionization of this $5p\pi$ orbital (93% p character) and, hence, tran-

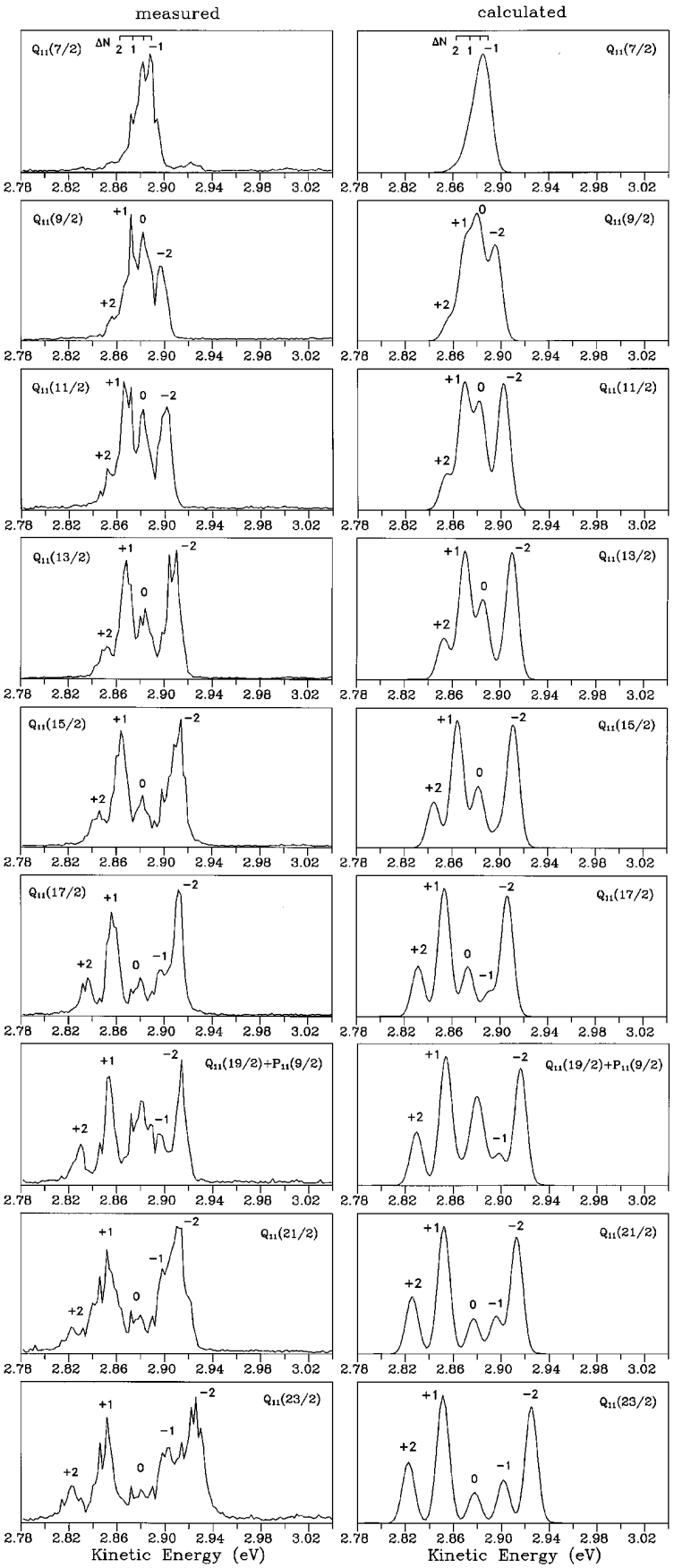

FIG. 5. The measured (left column) and calculated (right column) photoelectron spectra obtained in a $(2+1)$ photoionization process via the $Q_{11}(7/2)$ to $Q_{11}(23/2)$ rotational lines of the $[a\ ^1\Delta]3d\pi\ ^2\Phi \leftarrow\leftarrow X\ ^2\Pi$ two-photon transition of the SH radical leading to the $a\ ^1\Delta$ excited ionic state of the SH^+. The labeling denotes the changes in rotational angular momentum ΔN.

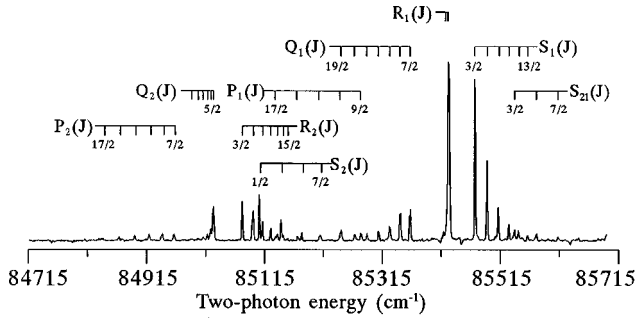

FIG. 6. The two-photon excitation spectrum of the SH radical in the two-photon energy range of 84 800–85 600 cm^{-1} obtained by only monitoring photoelectrons with a kinetic energy of approximately 4.2 eV. These electrons derive from a $(2+1)$ photon transition from the $X\ ^2\Pi(v''=0)$ ground state to the $a\ ^1\Delta(v^+=0)$ excited ionic state via the $[a\ ^1\Delta]5p\pi\ ^2\Phi$.

sitions up to $\Delta N=\pm 3$. However, our calculated photoelectron matrix elements also show a dominant f-wave contribution in addition to the expected s and d waves. For example, in Fig. 8, we show the magnitude of the (incoming-wave normalized) partial wave dipole amplitude $|D_l^{(-)}|$ as a function of photoelectron kinetic energy for the photoionization channels $5p\pi\rightarrow k\sigma$ [Fig. 8(a)], $5p\pi\rightarrow k\pi$ [Fig. 8(b)], and $5p\pi\rightarrow k\delta$ [Fig. 8(c)] via the $[a\ ^1\Delta]5p\pi\ ^2\Phi$ Rydberg state of SH. The photoionization of this $5p\pi$ orbital clearly carries much more of the signature of molecular scattering

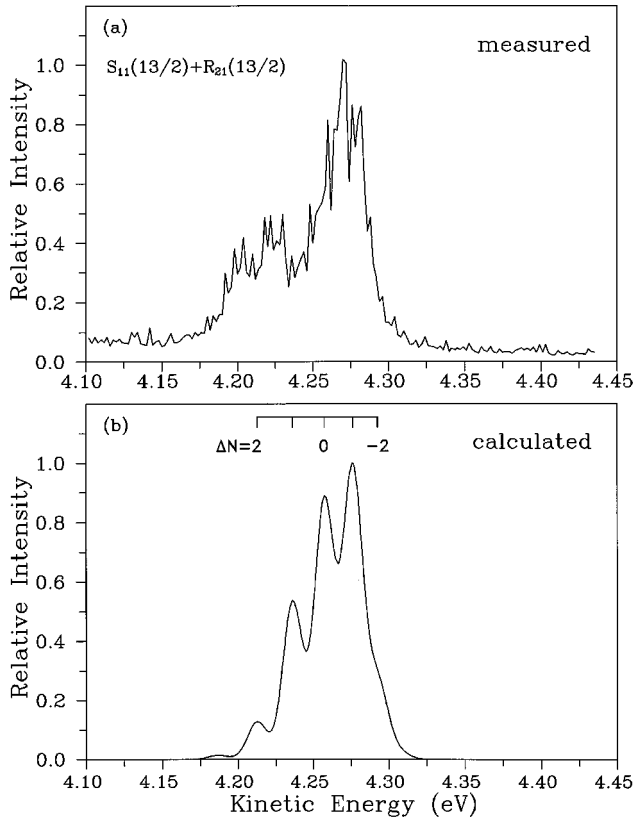

FIG. 7. The measured (a) and calculated (b) photoelectron spectra obtained in a $(2+1)$ REMPI photoionization process via the $S_{11}(13/2)+R_{21}(13/2)$ mixed rotational lines of the $[a\ ^1\Delta]5p\pi\ ^2\Phi(v'=0)\leftarrow\leftarrow X\ ^2\Pi$ two-photon transition of the SH radical leading to the $a\ ^1\Delta$ excited ionic state.

than photoionization of the $3d\pi$ orbital. Clearly, Eq. (17) cannot be used in cases where multiple partial waves contribute to the photoelectron matrix element, e.g., as in the $[a\ ^1\Delta]5p\pi\ ^2\Phi$ case here, at the kinetic energy of interest. Based on the conservation of angular momentum, up to $\Delta N=\pm 4$ transitions would be predicted for such a strong f-wave in the electronic continuum channels. The absence of such large angular momentum transfer suggests that interference between continuum channels also plays an important role here. The strong asymmetrical pattern seen here is again due to failure to reach the classical limit, as discussed above.

Figure 9 shows the measured [Fig. 9(a)] and calculated [Fig. 9(b)] photoelectron spectra obtained in a $(2+1)$ REMPI photoionization process via the $Q_{11}(17/2)+P_{21}(17/2)$ mixed rotational lines of the $[a\ ^1\Delta]5p\pi\ ^2\Phi(v'=0)\leftarrow\leftarrow X\ ^2\Pi$ two-photon transition of the SH radical leading to the $a\ ^1\Delta$ excited ionic state. The rotational level of this mixed branch is $N'=8$, which is the same as that of the mixed $S_{11}(13/2)+R_{21}(13/2)$ branch of Fig. 7. Therefore, the difference in spectral profile between them is due to the alignment in the rotational level of the intermediate $^2\Phi$ state induced by the two-photon excitation step. The most intense transition is the $\Delta N=0$ peak here, which differs from that for the $3d\pi$ case in which the $\Delta N=0$ transition is much weaker at the same rotational quantum number. The dominant $\Delta N=0$ transitions in both Figs. 7 and 9 indicate that the s wave contribution to the photoelectron matrix element is important, as shown in Fig. 8.

V. CONCLUSIONS

In this paper, we have studied the rotationally resolved photoelectron spectra for photoionization of the $[a\ ^1\Delta]3d\pi\ ^2\Phi$ and $[a\ ^1\Delta]5p\pi\ ^2\Phi$ Rydberg states of the SH radical leading to the $a\ ^1\Delta$ excited ionic state of SH^+ both experimentally and theoretically. Both Rydberg states reveal unusual photoionization dynamics, such as smaller changes in rotational angular momentum than expected, and asymmetrical patterns in the spectral ionization profiles. The strong asymmetries observed for both states underline the need for a full quantum mechanical description of the rotationally resolved photoionization process. On a more approximate level it appears that the sudden approach, which in most known cases is not very applicable, offers an adequate description of the photoionization dynamics of the $[a\ ^1\Delta]3d\pi\ ^2\Phi$ Rydberg state of SH. For the photoionization dynamics of the $[a\ ^1\Delta]5p\pi\ ^2\Phi$ Rydberg state, on the other hand, the molecular nature of this process needs to be considered explicitly.

ACKNOWLEDGMENTS

The group at the University of Amsterdam gratefully acknowledges the Netherlands Organization for Scientific Research (NWO) for equipment grants and for financial support (J.B.M.). Work at the California Institute of Technology was supported by grants from the Air Force Office of Scientific Research and the Office of Health and Environmental Research of the U.S. Department of Energy. We also ac-

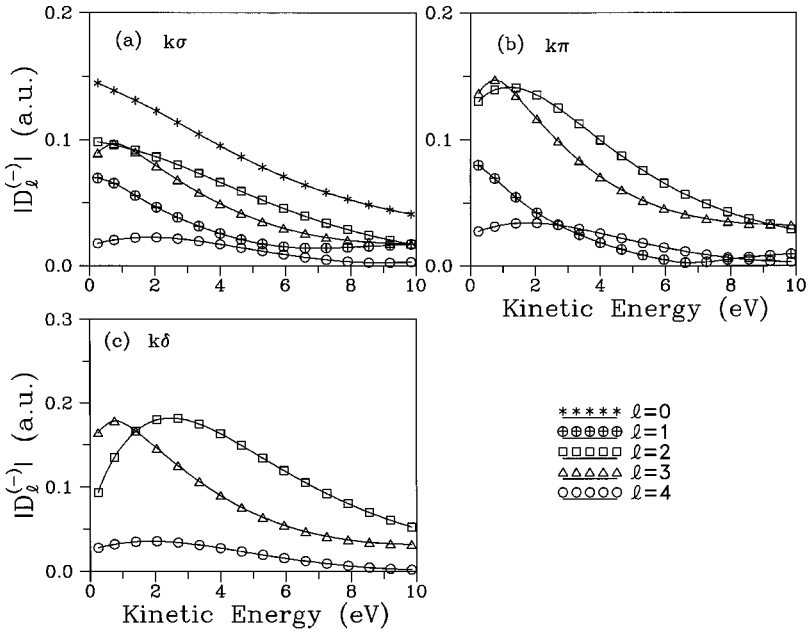

FIG. 8. Magnitude $|D_l^{(-)}|$ of the partial wave components of the photoelectron matrix element for photoionization of the $[a\ ^1\Delta]5p\pi\ ^2\Phi$ Rydberg state of SH for the (a) $5p\pi \rightarrow k\sigma$, (b) $5p\pi \rightarrow k\pi$, and (c) $5p\pi \rightarrow k\delta$ ionization channels.

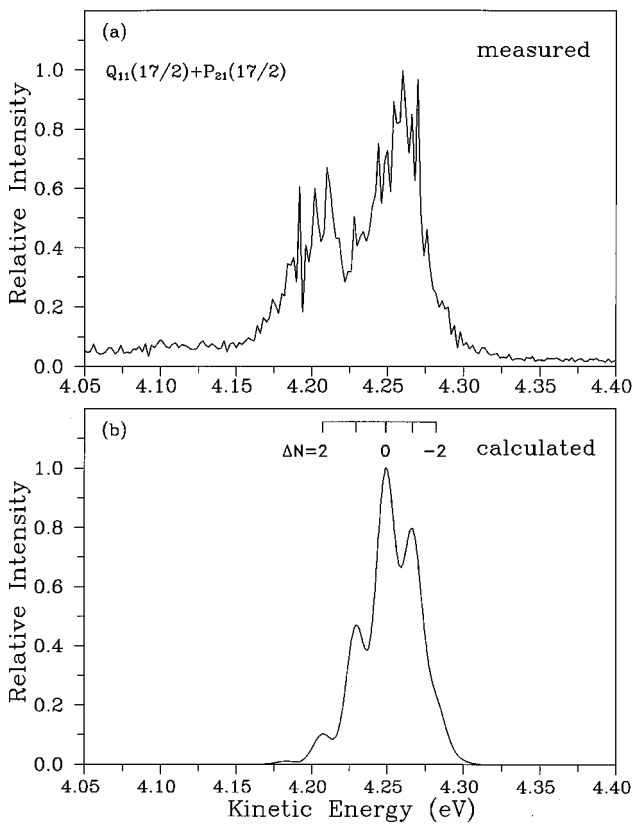

FIG. 9. The measured (a) and calculated (b) photoelectron spectra obtained in a (2+1) REMPI photoionization process via the $Q_{11}(17/2)+P_{21}(17/2)$ mixed rotational lines of the $[a\ ^1\Delta]5p\pi\ ^2\Phi(v'=0)\leftarrow\leftarrow X\ ^2\Pi$ two-photon transition of the SH radical leading to the $a\ ^1\Delta$ excited ionic state.

knowledge use of the resources of the Jet Propulsion Laboratory/California Institute of Technology CRAY Y-MP2E/232 supercomputer. Both groups gratefully acknowledge NATO for collaborative Grant No. CRG930183.

[1] K. P. Huber and G. Herzberg, *Molecular Spectra and Molecular Structure: IV. Constants of Diatomic Molecules* (Van Nostrand, New York, 1979).
[2] B. Morrow, Can. J. Phys. **44**, 2447 (1966).
[3] M. N. R. Ashfold, B. Tutcher, and C. M. Western, Mol. Phys. **66**, 981 (1989).
[4] K. Sinha, Proc. Astron. Soc. Aust. **9**, 32 (1991).
[5] M. L. Meeks, M. A. Gordon, and M. M. Litvak, Science **163**, 173 (1969).
[6] C. E. Heiles and M. B. E. Turner, Astrophys. Lett. **8**, 89 (1971).
[7] S. H. Ashworth and J. M. Brown, J. Mol. Spectrosc. **153**, 41 (1992).
[8] R. S. Ram, P. F. Bernath, R. Engleman, Jr., and J. W. Brault, J. Mol. Spectrosc. **172**, 34 (1995) and references therein.
[9] S. J. Dunlavey, J. M. Dyke, N. K. Farad, N. Jonathan, and A. Morris, Mol. Phys. **38**, 3 (1979); **44**, 265 (1981).
[10] C. W. Hsu, D. P. Baldwin, C. L. Liao, and C. Y. Ng, J. Chem. Phys. **100**, 8047 (1994).
[11] J. B. Milan, W. J. Buma, and C. A. de Lange, J. Chem. Phys. **104**, 521 (1996).
[12] S. G. Clement, M. N. R. Ashfold, C. M. Western, E. de Beer, C. A. de Lange, and N. P. C. Westwood, J. Chem. Phys. **96**, 4963 (1992).
[13] M. R. Dobber, W. J. Buma, and C. A. de Lange, J. Chem. Phys. **99**, 836 (1993).
[14] M. R. Dobber, W. J. Buma, and C. A. de Lange, J. Chem. Phys. **101**, 8303 (1994).
[15] R. A. Morgan, P. Puyuelo, J. D. Howe, M. N. R. Ashfold, W. J. Buma, N. P. L. Wales, and C. A. de Lange, J. Chem. Soc. Faraday Trans. **91**, 2715 (1995).
[16] M. R. Dobber, W. J. Buma, and C. A. de Lange, J. Phys. Chem. **99**, 1671 (1995).

[17] E. de Beer, M. P. Koopmans, C. A. de Lange, Y. Wang, and W. A. Chupka, J. Chem. Phys. **94**, 7634 (1991).
[18] E. de Beer, C. A. de Lange, J. A. Stephens, K. Wang, and V. McKoy, J. Chem. Phys. **95**, 714 (1991).
[19] E. de Beer, M. Born, C. A. de Lange, and N. P. C. Westwood, Chem. Phys. Lett. **186**, 40 (1991).
[20] K. Wang, J. A. Stephens, V. McKoy, E. de Beer, C. A. de Lange, and N. P. C. Westwood, J. Chem. Phys. **97**, 211 (1992).
[21] E. de Beer, C. A. de Lange, and N. P. C. Westwood, Phys. Rev. A **46**, 5653 (1992).
[22] N. P. L. Wales, E. de Beer, N. P. C. Westwood, W. J. Buma, C. A. de Lange, and M. C. van Hemert, J. Chem. Phys. **100**, 7984 (1994).
[23] J. D. Howe, M. N. R. Ashfold, R. A. Morgan, C. M. Western, W. J. Buma, J. B. Milan, and C. A. de Lange, J. Chem. Soc. Faraday Trans. **91**, 773 (1995).
[24] C. A. de Lange, in *High Resolution Laser Photoionization and Photoelectron Studies*, edited by I. Powis, T. Baer, and C. Y. Ng (Wiley, New York, 1995).
[25] J. B. Milan, W. J. Buma, C. A. de Lange, C. M. Western, and M. N. R. Ashfold, Chem. Phys. Lett. **239**, 326 (1995).
[26] J. B. Milan, W. J. Buma, and C. A. de Lange, J. Chem. Phys. **105**, 6688 (1996).
[27] J. B. Milan, W. J. Buma, C. A. de Lange, K. Wang, and V. McKoy, J. Chem. Phys. **103**, 3262 (1995).
[28] K. Wang, J. A. Stephens, and V. McKoy, J. Phys. Chem. **97**, 9874 (1993).
[29] K. Wang and V. McKoy, J. Chem. Phys. **95**, 4977 (1991).
[30] R. R. Lucchese, G. Raseev, and V. McKoy, Phys. Rev. A **25**, 2572 (1982).
[31] J. B. Halpern, H. Zacharias, and R. Wallenstein, J. Mol. Spectrosc. **79**, 1 (1980).
[32] S. N. Dixit and V. McKoy, Chem. Phys. Lett. **128**, 49 (1986).
[33] J. Xie and R. N. Zare, J. Chem. Phys. **93**, 3033 (1990).
[34] W. J. Hunt and W. A. Goddard, Chem. Phys. Lett. **3**, 414 (1969).
[35] A. D. McLean and G. S. Chandler, J. Chem. Phys. **72**, 5639 (1980).
[36] T. H. Dunning, J. Chem. Phys. **53**, 2823 (1970); **55**, 716, 3958 (1971).
[37] J. Xie and R. N. Zare, J. Chem. Phys. **97**, 2891 (1992).